

Hard X-ray morphology of the X1.3 April 25, 2014 partially occulted limb solar flare

Frederic Effenberger, Fátima Rubio da Costa and Vahé Petrosian

Department of Physics and KIPAC, Stanford University, Stanford, CA 94305, USA

E-mail: feffen@stanford.edu

Abstract. At hard X-ray energies, the bright footpoint emission from solar flare loops often prevents a detailed analysis of the weaker loop-top source morphology due to the limited dynamic range available for X-ray imaging. Here, we study the X1.3 April 25, 2014 flare with the *Reuven Ramaty High-Energy Solar Spectroscopic Imager (RHESSI)*. This partially occulted limb flare allows the analysis of the loop-top emission in isolation. We present results on the flare light curve at different energies, the source morphology from X-ray imaging and a detailed spectral analysis of the different source components by imaging spectroscopy. The loop-top source, a likely site of particle acceleration, shows a clear composition of different emission components. The results indicate the opportunities that detailed imaging of hard X-rays can provide to learn about particle acceleration, transport and heating processes in solar flares.

1. Introduction

Hard X-rays provide one of the most direct diagnostics for energetic particle processes in solar flares [1]. Studies in the past have shown that in some flares at least two distinct types of sources, namely from the coronal solar flare loop-top and chromospheric footpoints, can be distinguished [2, 3, 4, 5, 6, 7, 8, 9]. It is suggested by theory and observations that the coronal region at the loop-top is the main acceleration site for electrons (see, e.g. the review [10]). However, due to the limited dynamical range of *RHESSI* [11], it is often hard to clearly distinguish a coronal source, once strong footpoint emission is present. Partially occulted flares, in which the footpoints are a few degrees behind the solar limb, offer the opportunity to observe the coronal sources in isolation. Krucker & Lin [12] performed a statistical study of partially occulted flares during solar cycle 23. They concluded that thin-target radiation of electrons is a plausible scenario for the coronal emission. Some of the analyzed flares also show significant structure, indicating multiple coronal source regions. Kappa-distribution models [13, 14, 15] have been discussed as possible models for coronal X-ray sources, in particular if the sources are separated into different components, including an “above-the-loop-top” source.

Here, we focus on the X1.3 April 25, 2014 partially occulted limb flare, which shows a rich loop-top source morphology. Results on the flare light curve in different energies, the source structure from X-ray imaging, and a detailed spectral analysis of the different source components from imaging spectroscopy are presented. We note that this flare has also recently been studied in the context of CME initiation and a magnetic breakout scenario. See the paper by Chen et al. [16] for further details on these aspects.

2. Temporal evolution

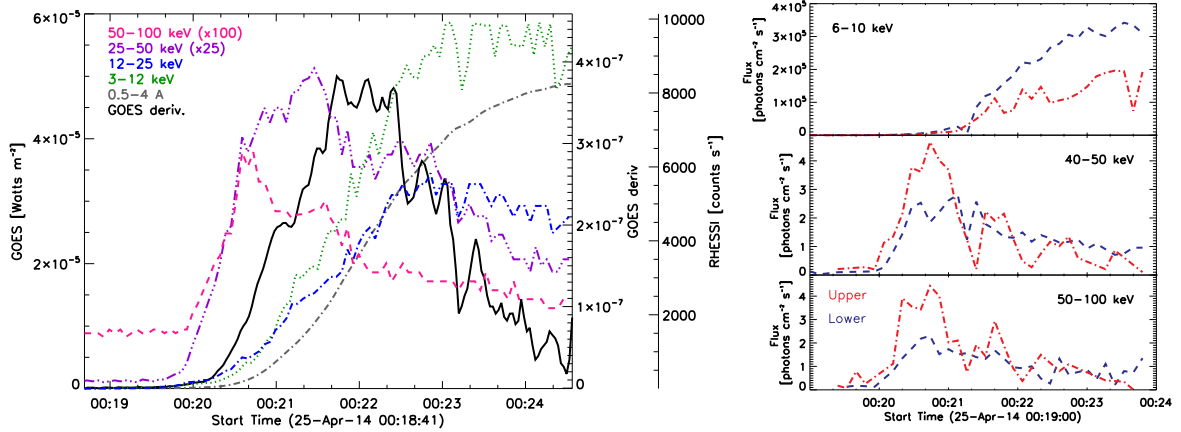


Figure 1. Upper left panel: Light curves of *RHESSI* count rates at four energy ranges (green, blue, purple and magenta), *GOES* high energy flux (0.4 to 4 Å, grey, dash-dotted) and its time derivative (black, solid). The counts in the two high energy channels are multiplied by 25 and 100, respectively, to make them comparable in magnitude. Right panel: Time evolution of photon flux in the two coronal regions selected (see the right panel of Figure 2), for three different energy channels.

We analyzed the temporal evolution of the hard X-ray flux for this flare and compared it with the *GOES* soft X-ray evolution in the high energy channel (0.4 to 4 Å). The left panel of Figure 1 gives an overview of the *RHESSI* light curve in four energy channels and the correlation with the *GOES* flux and its time derivative.

It can be seen that the two lowest energy channels are delayed with respect to the *GOES* derivative and are roughly correlated with the slow rise in *GOES* flux. The two high energy channels 25–50 keV and 50–100 keV, on the other hand, have an earlier and quicker rise to their maxima. In particular the 50–100 keV shows a prominent peak at the early onset and then a fast decay. A cross-correlation analysis showed the best correlation between the 25–50 keV channel and the *GOES* derivative, with a correlation coefficient of 0.81 and a lag of 12 s.

We note that a statistical study of more partially occulted events is currently in progress and a significant number of flares show better correlations and often small or zero lag. The implications of these results, in particular in the context of the so-called Neupert effect [17, 18], will be discussed elsewhere.

The right panel of Figure 1 shows the photon flux evolution in two different regions of the coronal source, namely an upper and lower part. The regions are defined in the right panel of Figure 2. We see that there is a faster rise at high energies in the upper part of the coronal source resulting in a stronger maximum. The lower energy fluxes slowly rise to larger values for the lower source. We now turn to the details of the source structure in X-ray images.

3. Hard X-ray Imaging

RHESSI's unique imaging capability allows a detailed study of the spatial structure of the hard X-ray emission. In Figure 2, we present the evolution over four subsequent time intervals of 12 s length. The X-ray contours, obtained using the CLEAN algorithm [19], at three different energies are overlaid over AIA 131 Å background images closest in time to the *RHESSI* integration time interval (start times given above the images). An expanding upper loop structure can be detected in the AIA images, associated to a high energy (50–100 keV) upper source moving outwards.

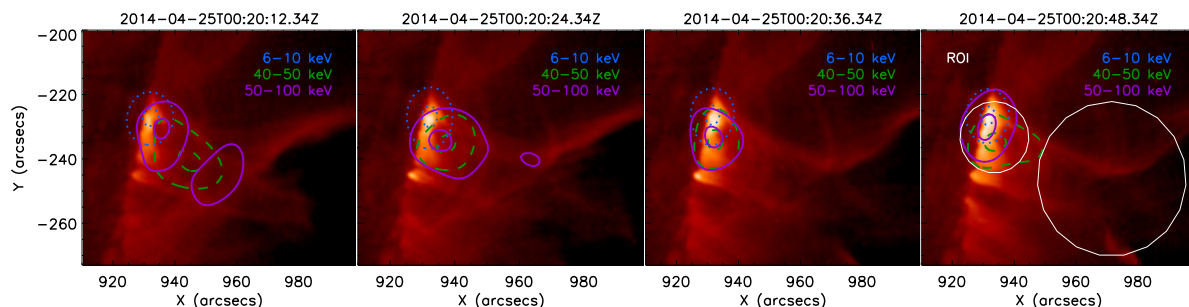


Figure 2. Time evolution of the X1.3 April 25, 2014 flare in AIA 131 Å with *RHESSI* contours at different energy ranges (77% and 97% of the maximum intensity at each time, applying the CLEAN algorithm): 6-10 keV (dotted blue), 40-50 keV (dashed green) and 50-100 keV (solid purple). The rightmost panel also indicates the two selected ROI for the imaging spectroscopy analysis of Section 4.

The high energy (up to 100 keV), non-thermal loop-top emission comes mainly from the upper region of the X-ray source, while the thermal 6-10 keV emission is much stronger in the lower parts of the loops. We note that no quasi-footpoint emission is detected, confirming that the flare is partially occulted and that we are seeing a simultaneously observed loop-top and a second higher above-the-loop-top source (see, e.g., [20, 21, 22]). These uncommon observations allow us to separate the upper and lower coronal emission for further studies. To this end, we performed an imaging spectroscopy study discussed next.

4. Imaging spectroscopy

Thanks to the high energy and spatial resolution of *RHESSI*, it is possible to obtain X-ray spectra of different separated regions. In order to study the spectral evolution of the two sources, we defined two regions of interest (ROI), indicated as white circles in the right panel of Figure 2. We obtained photon spectra of the two different regions resulting from the CLEAN images of these regions.

The red and blue data points of Figure 3 give the results for the upper and lower sources, respectively, at four different times. The spectra are fitted to a thin-target model with a power law electron energy spectrum. The resulting electron spectral index δ is reported in the bottom part of the figures. In general, the upper source has a harder high energy spectrum.

The fit derived from the thin target model is in good agreement with the data in all cases. We note that a thick-target model is often not an appropriate model for coronal sources, due to the low column depth of gas in the source (see, however, [23]). In particular, the relevant time scales of particle escape and energy loss in the loop source are often such that particles tend to lose only a fraction of their energy before they escape. This was found in the study by Chen & Petrosian [24] for an X3.9 and an M2.1 on disk flares, where these time scales could be determined non-parametrically with an inversion procedure.

A thin-target kappa function fit [13] to the photon spectra gives, as should be expected, almost identical values for κ and δ . This is due to the fact that κ is defined to be the parameter in the number density distribution while δ is the index of the electron flux density distribution, see the discussion in [14]. We do not show these fit results since they look very similar to Figure 3.

To gain an additional perspective on the spectral properties of electrons, we obtained electron images and spectra directly using a regularized imaging inversion method [25]. The resulting electron images (not shown) display a similar upward motion of the upper source as in the photon images. The electron spectra for the same ROI are shown in Figure 4, and were fitted

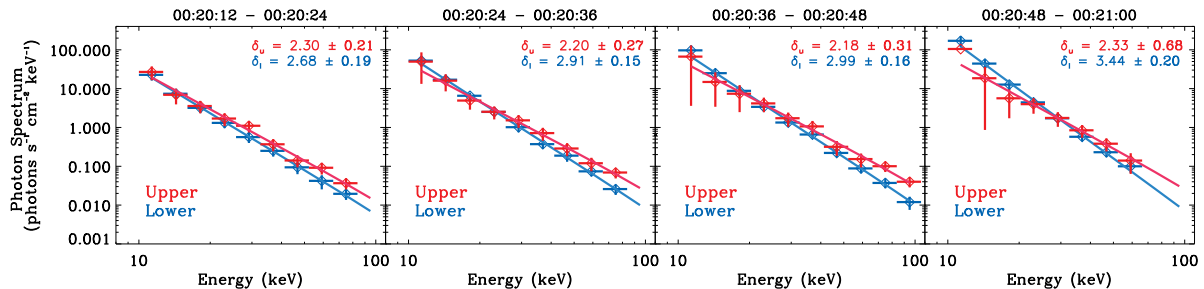


Figure 3. Photon spectra at the same four time ranges as in Figure 2 for the two separate ROI (red: upper source, blue: lower source). The spectra have been fitted to a thin-target model based on a broken power-law. The parameter values of the fit are given in the lower parts of the panels.

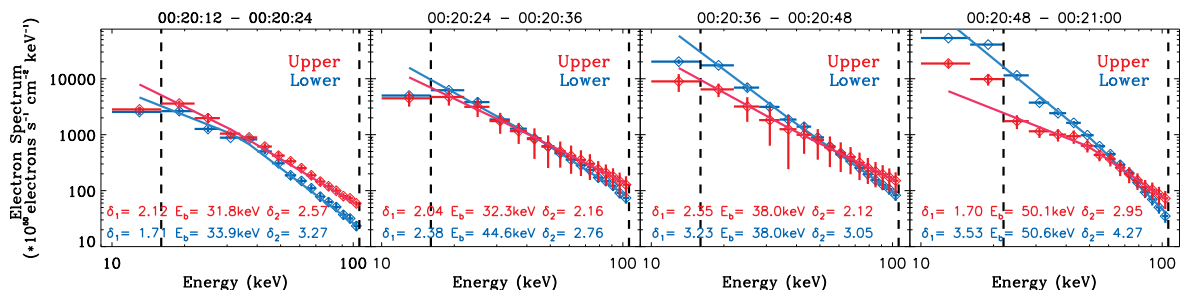


Figure 4. Similar to Figure 3, but now as electron spectra resulting from the regularized imaging inversion with the same ROI. The spectra have been fitted to a broken power-law, with the parameter values of the fit reported in the lower parts of the panels.

to a broken power-law. We see that there is significant electron flux at high energies, with clear power-laws extending to up to ~ 100 keV, for both source regions. Considering that the errors in the fitting parameters are of the same order as in the previous thin-target fit, the upper source has generally slightly harder spectral indices and higher fluxes at high energies, pointing at a possibly more effective acceleration mechanism in this part of the loop. Most of the spectra are compatible with a single power-law, in particular for the two time intervals in the middle.

Taking into account the confidence intervals for the photon spectra thin target fitting parameters, as stated in Figure 3, we find that the resulting electron spectra are in reasonable agreement for both methods. This confirms the notion of thin-target emission for the entire coronal source region and gives independent support to the different spectral characteristics of the two parts of the source.

5. Conclusions

We have analyzed the X1.3 April 25, 2014 partially occulted limb flare in hard X-rays with *RHESSI* imaging and spectroscopy. The coronal emission shows a rich morphology with at least two different coronal source regions. The upper source is moving upwards and detaching from the lower source during the flare evolution over a short time interval of tens of seconds (see also [26, 27] for similar observations of other flares).

We found a different electron spectral behavior in the upper and lower source derived from a forward thin-target fit and regularized imaging inversion. The differences between the results obtained with the two methods are mostly within the error bounds. The upper source has somewhat smaller (harder) spectral indices than the lower source. Different scenarios could

explain this result. Assuming the reconnection region lies between these two source regions, the effective distance to the reconnection region could imply different turbulence levels. This in turn can result in harder (higher turbulence level) or softer (lower turbulence level) electron spectra for the accelerated population [20, 28].

For further insights into the differences of coronal source modeling and electron properties, a larger sample of partially occulted flares needs to be studied. Detailed comparisons with simulations of particle acceleration and transport will help to uncover the acceleration mechanisms at work in different parts of the flare loop.

Acknowledgments

The authors thank S. Krucker for suggesting the combined *RHESSI* and *GOES* light-curve analysis. F.E. thanks the organizers and participants of the 15th Annual International Astrophysics Conference for the stimulating discussions. This work was supported by NASA grants NNX14AG03G and NNX13AF79G.

References

- [1] Fletcher L, Dennis B R, Hudson H S *et al.* 2011 *Space Sci. Rev.* **159** 19–106
- [2] Frost K J and Dennis B R 1971 *ApJ* **165** 655
- [3] Roy J R and Datlowe D W 1975 *Sol. Phys.* **40** 165–182
- [4] McKenzie D L 1975 *Sol. Phys.* **40** 183–191
- [5] Hudson H S 1978 *ApJ* **224** 235–240
- [6] Masuda S, Kosugi T, Hara H, Tsuneta S and Ogawara Y 1994 *Nature* **371** 495–497
- [7] Petrosian V, Donaghy T Q and McTiernan J M 2002 *ApJ* **569** 459–473
- [8] Krucker S, White S M and Lin R P 2007 *ApJ* **669** L49–L52
- [9] Simões P J A and Kontar E P 2013 *A&A* **551** A135
- [10] Petrosian V 2012 *Space Sci. Rev.* **173** 535–556
- [11] Lin R P, Dennis B R, Hurford G J *et al.* 2002 *Sol. Phys.* **210** 3–32
- [12] Krucker S and Lin R P 2008 *ApJ* **673** 1181–1187
- [13] Kašparová J and Karlický M 2009 *A&A* **497** L13–L16
- [14] Oka M, Ishikawa S, Saint-Hilaire P, Krucker S and Lin R P 2013 *ApJ* **764** 6
- [15] Bian N H, Emslie A G, Stackhouse D J and Kontar E P 2014 *ApJ* **796** 142
- [16] Chen Y, Du G, Zhao D, Wu Z, Liu W, Wang B, Ruan G, Feng S and Song H 2016 *ApJ* **820** L37
- [17] Neupert W M 1968 *ApJ* **153** L59
- [18] Veronig A M, Brown J C, Dennis B R, Schwartz R A, Sui L and Tolbert A K 2005 *ApJ* **621** 482–497
- [19] Hurford G J, Schmahl E J, Schwartz R A *et al.* 2002 *Sol. Phys.* **210** 61–86
- [20] Liu W, Petrosian V, Dennis B R and Jiang Y W 2008 *ApJ* **676** 704–716
- [21] Liu W, Chen Q and Petrosian V 2013 *ApJ* **767** 168
- [22] Oka M, Krucker S, Hudson H S and Saint-Hilaire P 2015 *ApJ* **799** 129
- [23] Fleishman G D, Xu Y, Nita G N and Gary D E 2016 *ApJ* **816** 62
- [24] Chen Q and Petrosian V 2013 *ApJ* **777** 33 (*Preprint* 1307.1837)
- [25] Piana M, Massone A M, Hurford G J, Prato M, Emslie A G, Kontar E P and Schwartz R A 2007 *ApJ* **665** 846–855
- [26] Sui L and Holman G D 2003 *ApJ* **596** L251–L254
- [27] Sui L, Holman G D and Dennis B R 2004 *ApJ* **612** 546–556
- [28] Petrosian V and Liu S 2004 *ApJ* **610** 550–571